Dynamical Transition in the Wigner Solid on a Liquid Helium Surface

Keiya Shirahama and Kimitoshi Kono

Institute for Solid State Physics, University of Tokyo, Roppongi 7-22-1, Minato-ku, Tokyo 106, Japan

(Received 29 July 1994)

We have observed a dynamical transition in the Wigner solid on liquid ^{4}He. The ac Corbino conductivity σ_{xx} jumps abruptly at certain input voltage and shows hysteretic behavior. The threshold input voltage $V_{\rm th}$ has dependences on the magnetic field B perpendicular to the surface, frequency ω, electron density n_s, and electric field $E_\perp$ as $V_{\rm th} \propto B^{-0.8}\omega^{-1}n_s^{1.5}E_\perp$. We attribute the conductivity jump to the collective sliding of the electrons out of the periodic deformation of the He surface.

PACS numbers: 73.20.Dx, 67.40.Hf, 73.50.Fq

Electrons trapped on the liquid He surface constitute a unique two-dimensional system [1]. Since the He surface is smooth and has no impurities, it realizes extremely high mobility, even over 10^8 cm^2/V sec [2], and behaves as an ideal nondegenerate electron system. The most prominent phenomenon is a transition to the Wigner solid (WS) phase, in which the electrons form a triangular lattice. The WS on liquid He is accompanied with the periodic surface deformation whose wave vectors equal the reciprocal lattice vectors of the crystal. Since the deformation comes from the static part of the coupled plasmon-ripplon (CPR) modes [3], we refer hereafter to the WS state accompanied with the surface deformation as the CPR state. The first identification of the WS was made by observing the CPR resonance [4]. In this Letter, we report the observation of a dynamical transition in the WS on the liquid ^{4}He surface. The transition appears as an abrupt jump of the electron conductivity with changing the external ac field. We attribute the transition to a collective sliding of the electrons out of the periodic surface deformation; the transition from the CPR state to the sliding state of the WS.

We have conducted an accurate measurement of the diagonal component of the ac conductivity tensor, σ_{xx}. We employ a capacitive coupling method, which was first developed by Sommer and Tanner [5]. A concentric-ring copper electrode pair, which is known as the Corbino disk, is set 1 mm beneath the He surface. The inner and outer diameters are 20 and 30 mm, respectively, and the gap between them is about 0.1 mm. The electrons are generated at 1.4 K by thermionic emission of a tungsten filament, which is located 2 mm above the liquid. The electrodes are biased at a positive voltage $V_{\rm dc}$, and the electron density n_s is determined by the shielding condition of the electric field above the liquid, $n_s = \epsilon V_{\rm dc}/4\pi ed$, where ϵ is the dielectric constant of liquid ^{4}He, and d the depth of the liquid. The data reported here are taken at the electron density $n_s = 1.08 \times 10^8$ cm^{-2} unless otherwise specified. A circular brass guard electrode surrounds the electrons, which is kept at -1.5 V to confine the electrons radially. The electrode assembly is enclosed in a copper cell, which is mounted on a dilution refrigerator.

To measure σ_{xx}, an ac voltage $V_{\rm in}$ of 100 kHz is superimposed to the inner electrode. The current is detected from the outer electrode, which is capacitively coupled to the electrons, as a voltage induced on both ends of a capacitor $C_{\rm out}$, which is connected between the outer electrode and the ground. We apply a static magnetic field B perpendicular to the surface. The in-phase and quadrature components of the output voltage $V_{\rm out}$ are monitored by a vector lock-in amplifier. We obtain σ_{xx} by fitting $V_{\rm out}$ with a formula given by [6,7]

$$\frac{V_{\rm out}}{V_{\rm in}} = \pi^2 r_i^2 \frac{C^2}{(C + C')C_{\rm out}} f(\beta, r_o, r_i), \qquad (1)$$

where

$$f(\beta, r_o, r_i) = \frac{J_1(\beta r_i)}{J_1(\beta r_o)} \times [N_1(\beta r_o)J_1(\beta r_i) - J_1(\beta r_o)N_1(\beta r_i)],$$

and $\beta = \sqrt{-i\omega\sigma_{xx}^{-1}(C + C')}$. Here r_o and r_i are the outer and inner radii of the Corbino disk, respectively. C denotes the sheet capacitance between the electrons and the Corbino electrodes, whereas C' is the one between the electrons and the upper cell wall. J_1 and N_1 are the Bessel and Neumann functions of first order, respectively.

The inset (a) of Fig. 1 shows the temperature dependence of σ_{xx} at $B = 261$ G for 2.0 mV$_{\rm p.p.}$ (peak-to-peak) input voltage. We identify the Wigner transition as an abrupt increase of σ_{xx} at 220 mK. This melting temperature is consistent with the generally accepted value of the critical plasma parameter, $\Gamma_c = 127$. Note that the increase of σ_{xx} under the Corbino geometry corresponds to the decrease of the mobility μ.

In Fig. 1, we show the typical behavior of σ_{xx}^{-1} of the WS, as a function of the input voltage $V_{\rm in}$. At about 5 mV$_{\rm p.p.}$, σ_{xx}^{-1} shows a maximum, then decreases. This strongly non-Ohmic behavior is observed only in the WS. Increasing $V_{\rm in}$ further, σ_{xx}^{-1} tends to a constant and *jumps abruptly*. The fluctuation increases above the jump. In the downward sweep, σ_{xx}^{-1} does not follow the same path as the upward one, and the jump occurs at lower $V_{\rm in}$ than the upward sweep case. Below the σ_{xx} jump, the upward and downward sweeps follow the same trace. Both the upward and downward threshold voltages

0031-9007/95/74(5)/781(4)$06.00

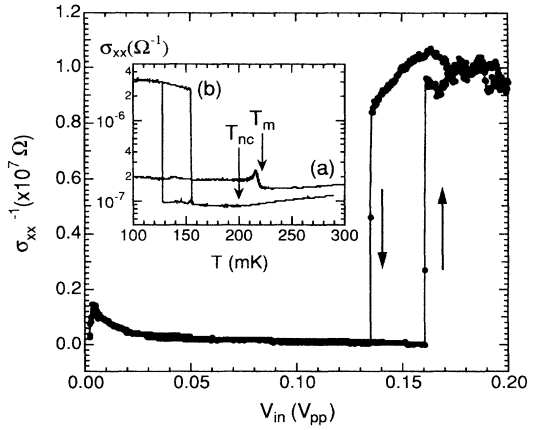

FIG. 1. σ_{xx}^{-1} as a function of driving voltage $V_{\rm in}$, at T = 80 mK and B = 217 G. Arrows indicate the direction of the sweep. Inset: σ_{xx} as a function of temperature. (a) $V_{\rm in}$ = 2.0 $mV_{p.p.}$ and B = 289 G. (b) $V_{\rm in}$ = 100 $mV_{p.p.}$ and B = 317 G. T_m and $T_{\rm nc}$ denote the Wigner melting and the non-CPR transition, respectively (see text).

vary from run to run, but are located within about 10%. Near the thresholds, the electrons are very sensitive to the external disturbance, e.g., the mechanical vibration of the cryostat easily triggers the jump. It should be emphasized that the electrons become more *mobile* above the thresholds.

The most striking feature in the σ_{xx} jump is its power law dependences on such quantities as the applied magnetic field, pressing electric field, driving frequency, and electron density. In Fig. 2, we show the threshold voltage $V_{\rm th}$ as a function of B for three temperatures. Although the jump is hysteretic, $V_{\rm th}$'s collapse onto a straight line very well in the log-log plot, so it obeys a power law, $V_{\rm th} \propto B^{\zeta}$. The exponent ζ is about -0.8. The hysteresis is largest at the intermediate field, and it becomes less prominent as B increases. Approaching the melting temperature T_m, $V_{\rm th}$ decreases and deviates from the power law at high field. The jump disappears at T_m.

One can control the electron-ripplon coupling by changing the bias voltage $V_{\rm dc}$, i.e., the electric field $E_\perp$ which presses the electrons toward the liquid. To study the influence of the pressing field on the σ_{xx} jump, we measure $V_{\rm th}$ for various $E_\perp$'s while keeping n_s constant. The results are shown in Fig. 3. We find definitely that $V_{\rm th}$ is a linear function of $E_\perp$.

$V_{\rm th}$ depends also on the frequency ω and electron density n_s. From 10 up to 150 kHz, $V_{\rm th}$ is almost inversely proportional to ω. Above 200 kHz, $V_{\rm th}$ deviates from the ω^{-1} dependence and tends to be independent of ω, and the threshold fades. From the $E_\perp$ dependence such as in Fig. 3 for various n_s's we obtain the n_s dependence of $V_{\rm th}$ by picking up $V_{\rm th}$'s at the same $E_\perp$. This analysis yields the result $V_{\rm th} \propto n_s^{1.5}$. Our observation of $V_{\rm th}$ is summarized as follows:

$$V_{\rm th} \propto B^{-0.8}\omega^{-1}n_s^{1.5}E_\perp . \qquad (2)$$

While preparing this Letter, we became aware that the similar σ_{xx} jump was observed previously by Giannetta and Wilen [8]. They found the σ_{xx} jump in the magnetic field sweep for various drive voltages. The phenomena which they found seem the same as what we have observed here. They interpreted the σ_{xx} jump as the nonequilibrium melting of the WS, caused by the magnetic field induced shear. We believe that the nonequilibrium melting is not an adequate interpretation of the σ_{xx} jump, because their model can never explain the strong *frequency dependence* of the threshold. We give a simple model, which explains systematically the dependences of

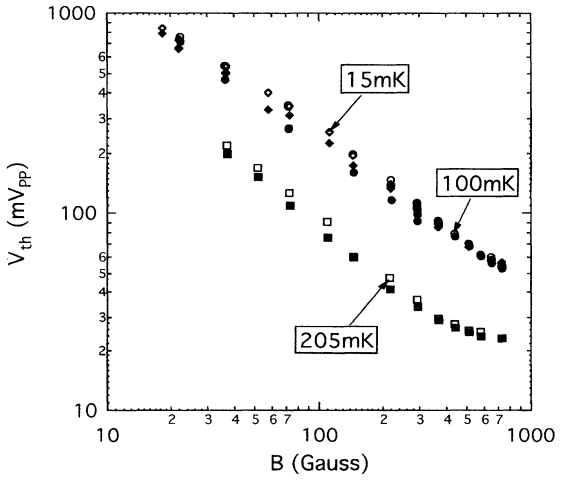

FIG. 2. Threshold voltage $V_{\rm th}$ as a function of magnetic field B. The filled symbol denotes $V_{\rm th}$ in the upward sweep, while the open one is for the downward case. Lozenges, 15 mK; circles, 100 mK; squares, 205 mK.

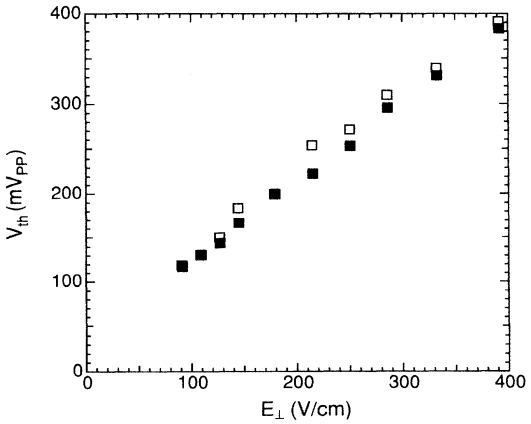

FIG. 3. $V_{\rm th}$ plotted as a function of the pressing electric field $E_\perp$, at T = 15 mK and B = 724 G. Open and filled squares indicate the upward and downward drive sweeps, respectively.

V_{th} on various quantities including the frequency, on the basis of the sliding concept in the following.

In equilibrium, the electrons are positioned at each bottom of the periodic, approximately sinusoidal, deformation of the surface [3,9]. In the presence of the electron-ripplon interaction, the deformation causes a spatial corrugation of the potential energy for the electrons, having the same sinusoidal form as the surface deformation itself. In the σ_{xx} measurement, the ac driving field tilts the potential as a whole. For the field at which the local potential minima disappear, the electrons can move on in the tilted potential, i.e., the electrons *slide*. This results in the observed abrupt jump of σ_{xx}. To some extent the situation is analogous to the rigid-body model of a sliding charge-density wave (CDW) [10].

The magnetic field applied perpendicular to the surface leads to two important effects. (1) In the Corbino geometry, the magnetic field enhances effectively the driving electric field. (2) If the scattering is negligible, the electrons drift along the contours of the deformation potential.

In the capacitive-coupling method, the ac drive applied to the inner electrode causes the inhomogeneity of the electric field in the cell. The electrons flow so as to cancel this field inhomogeneity, i.e., the current is caused by the *shielding* effect. Since the magnetic field decreases σ_{xx}, the shielding by the surface electrons is thereby *weakened*. The higher the magnetic field, the stronger the inhomogeneity of the electric field in the WS. We see that a higher magnetic field keeps the potential slope steeper, and hence lowers more the sliding threshold voltage.

Ignoring the scattering, the Lorentz force drifts the electrons along the contours of the potential. As long as the driving field is so weak that the potential minima exist, each electron localizes on the closed contours around each potential minimum. When the minima disappear, all the contours are no longer closed, but *extend outside,* and the electrons can slide without limit. Therefore, even in the presence of the magnetic field, the disappearance of the potential minima gives the appropriate criterion for the electron sliding.

So far we have implicitly assumed that the deformation potential is rigid. This can be justified under the condition that the electron velocity exceeds the phase velocity of ripplons [3]. We find that, in our experiment, the maximum velocity of the WS at the threshold exceeds the ripplon phase velocity by a factor of 4. Therefore, we may assume the rigid potential in our experimental condition. Once the electrons start to slide, the original deformation disappears, because the ripplons cannot follow the fast electron motion. This situation is quite different from the case of the sliding CDW, and offers a new aspect in general sliding phenomena.

With the sliding concept we discuss the threshold. The maximum restoring force for the electron in the deformation is given by [3,11]

$$F_{\mathrm{rmax}} \sim \frac{n_s}{\sigma}(eE_\perp + U_{G_1})^2 (n^0_{G_1})^2 \frac{\gamma}{G_1}, \tag{3}$$

where σ is the surface tension of ^{4}He, G_1 the shortest reciprocal lattice vector, the "electron form factor" n^0_G is expressed in terms of the Debye-Waller factor W as e^{-2W}, and γ is an orientation dependent constant of about 3. The polarization term U_G here is so small that we could neglect it.

The external driving force is given by $F_d = -e^2 n_s v \sigma_{xx}^{-1}$, where v is the electron velocity, which is obtained in the course of the derivation of Eq. (1). The maximum driving force F_{dmax} results at the gap of the electrodes, and is obtained as

$$F_{\mathrm{dmax}} = \left| \frac{\pi r_i}{2} e\omega C \sigma_{xx}^{-1} f(\beta, r_o, r_i) V_{\mathrm{in}} \right| . \tag{4}$$

We may regard $f(\beta, r_o, r_i)$ as a constant of order unity so far as σ_{xx} just below the threshold is concerned. The σ_{xx} jump occurs when F_{dmax} exceeds F_{rmax}. From this condition, the following expression for V_{th} emerges,

$$|V_{\mathrm{th}}| \propto \frac{n_s \sigma_{xx} (n^0_{G_1})^2}{\omega G_1} E_\perp^2 . \tag{5}$$

From Eq. (5), we see the following: (1) V_{th} is inversely proportional to ω, providing that σ_{xx} is independent of ω; (2) because G_1 is proportional to $\sqrt{n_s}$ and σ_{xx} is proportional to n_s, V_{th} is proportional to $n_s^{1.5}$; (3) the form factor $n^0_{G_1}$ makes V_{th} vanish at the WS melting, cf. Fig. 4. These conclusions, in particular (1) and (2), immediately explain part of the experimental results for V_{th}, Eq. (2). The other relations, $V_{\mathrm{th}} \propto B^{-0.8} E_\perp$, are not obvious from Eq. (5). In

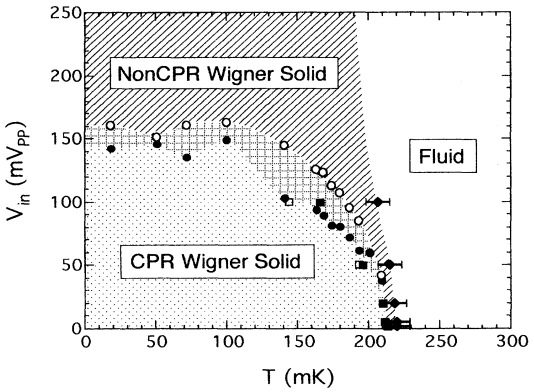

FIG. 4. V_{in}-T phase diagram at $B = 217$ G and $E_\perp = 92.5$ V/cm. Open and filled circles are V_{th}'s for the upward and downward sweeps at fixed temperatures, respectively. Open and filled squares are the ones, respectively, for the downward and upward temperature sweeps with fixed drive. The transition region is indicated by a checked pattern. Lozenges denote T_{nc}'s (see text). Plain, dotted, and hatched regions indicate the fluid, the CPR state, and the non-CPR state, respectively.

the fluid phase where the Drude law holds, σ_{xx} is approximately $n_s e/\mu B^2$ in a strong magnetic field. Moreover, μ in the ripplon limited regime is proportional to $E_\perp^{-2}$. If the Drude law held also in the WS, Eq. (5) would give larger exponents for the B and $E_\perp$ dependences than the observed ones. However, we have in fact found that σ_{xx} in the WS is inversely proportional to B and $E_\perp$. The origin of this peculiar behavior of the WS has not been understood. Detailed studies for this interesting subject are under way. From Eq. (5) and $\sigma_{xx} \propto B^{-1}E_\perp^{-1}$, we obtain the relation $V_{\rm th} \propto B^{-1}E_\perp$. The B dependence is fairly close to the observed one, i.e., $B^{-0.8}$, and the $E_\perp$ dependence agrees well with the experimental result.

To check our model quantitatively, we estimate $F_{\rm rmax}$ and $F_{\rm dmax}$ at the threshold from Eqs. (3) and (4). The result is that $F_{\rm dmax}$ is roughly 6 times as large as $F_{\rm rmax}$. The sliding criterion, that $F_{\rm dmax}$ exceeds $F_{\rm rmax}$, is satisfied. Further quantitative comparison of $F_{\rm dmax}$ and $F_{\rm rmax}$ will be made by considering self-consistently the effect of the distortion of the potential to the CPR dynamics. We conclude that the rigid-body sliding model gives a fairly good explanation for the principal experimental observations of the dynamical transition.

From the dependences of $V_{\rm th}$ on T, B, $E_\perp$, and n_s, we can draw a phase diagram in $V_{\rm in}$-T-B-$E_\perp$-n_s space. A $V_{\rm in}$-T section of the phase diagram at $B = 217$ G, $E_\perp = 92.5$ V/cm is shown in Fig. 4. As suggested in Fig. 2, $V_{\rm th}$ decreases as T approaches T_m. At low $V_{\rm in}$ and low T, the CPR state is formed. It is interesting to elucidate whether the WS melts above $V_{\rm th}$. To see this, in the inset (b) of Fig. 1, we show the σ_{xx} taken at $V_{\rm in} = 100$ $\rm mV_{p.p.}$ and at 317 G. As T decreases, σ_{xx} decreases down to 200 mK. This is the same behavior as in the 2.0 $\rm mV_{p.p.}$ data and reflects that the electrons are in the fluid phase and scattered from ripplons. Below 200 mK, slightly lower than T_m identified by the 2.0 $\rm mV_{p.p.}$ measurement, σ_{xx} begins to increase again with lowering temperature. Eventually the abrupt σ_{xx} jump, which is the transition to the CPR state, occurs at 128 mK. We speculate that the small change of σ_{xx} at 200 mK indicates the transition to the Wigner solid which is decoupled from the surface deformation. We may call it a non-CPR state. In Fig. 4, we show the possible non-CPR state by plotting the temperature $T_{\rm nc}$ where σ_{xx} changes the temperature dependence. $T_{\rm nc}$ slightly decreases with increasing $V_{\rm in}$. Studies such as plasma resonance will shed further light on the nature of this new state.

In conclusion, we have found that the strong ac electric field in the Corbino configuration causes a unique dynamical transition in the Wigner solid on the He surface. The transition is assigned to the sliding of the WS out of the surface deformation. Our observation has revealed that the electron-ripplon coupling makes the WS dynamics strongly nonlinear. The WS on the liquid He will offer an interesting example for the study of nonlinear phenomena.

We are grateful to S. Ito for his experimental help. K. S. is supported by Grant-in-Aid for Encouragement of Young Sciencists from the Ministry of Education, Science and Culture of Japan.

[1] For reviews, see C. C. Grimes, Surf. Sci. **73**, 379 (1978); F. I. B. Williams, *ibid.* **113**, 371 (1982).
[2] K. Kono, S. Ito, and K. Shirahama (to be published).
[3] D. S. Fisher, B. I. Halperin, and P. M. Platzman, Phys. Rev. Lett. **42**, 798 (1979).
[4] C. C. Grimes and G. Adams, Phys. Rev. Lett. **42**, 795 (1979).
[5] W. T. Sommer and D. J. Tanner, Phys. Rev. Lett. **27**, 1345 (1971).
[6] R. Mehrotra and A. J. Dahm, J. Low Temp. Phys. **67**, 115 (1987).
[7] K. Kono, U. Albrecht, and P. Leiderer, J. Low Temp. Phys. **82**, 279 (1991). In this paper there are typographical errors. Zeroth-order Bessel and Neumann functions stand for the first-order ones.
[8] R. Giannetta and L. Wilen, Solid State Commun. **78**, 199 (1991). We thank M. J. Lea and R. W. van der Heijden for pointing out this work.
[9] Yu. P. Monarkha and V. B. Shikin, Sov. Phys. JETP **41**, 710 (1975); V. B. Shikin, *ibid.* **45**, 850 (1977).
[10] G. Grüner, A. Zawadowski, and P. M. Chaikin, Phys. Rev. Lett. **46**, 511 (1981).
[11] A-M. Trembray and V. Ambegaokar, Phys. Rev. B **20**, 2190 (1979).